Aeroacoustics Conferences
June 14-17, 2022, Southampton, UK
28th AIAA/CEAS Aeroacoustics 2022 Conference

10.2514/6.2022-3103

Towards a semi-empirical trailing edge noise model valid for attached and separated turbulent boundary layers

Benjamin Cotté *, Sayahnya Roy†, David Raus‡, Rayan Oueini§.
Institute of Mechanical Sciences and Industrial Applications (IMSIA), ENSTA Paris, CNRS, CEA, EDF, Institut Polytechnique de Paris, France

The present work investigates the noise radiated by an airfoil over a large range of angles of attack, for which the boundary layer can be attached or partially separated. We propose a trailing edge noise model based on Amiet's theory, where the spanwise coherence length and the wall pressure spectrum are evaluated based on semi-empirical models. The model predictions are compared to wall pressure and far-field acoustic measurements performed in an anechoic wind tunnel on a NACA$63_3$418 airfoil. At low angles of attack, where the boundary layer is attached, the best predictions are obtained with the Smol'yakov model for the spanwise coherence length, and the Rozenberg-Lee model for the wall pressure spectrum in the presence of an adverse pressure gradient. At higher angles of attack, where the boundary layer is partially separated, Bertagnolio's model predicts relatively well the wall pressure spectrum when the separation point is estimated from the measured static pressure distribution, but underestimates the spanwise coherence length.

I. Introduction

Wind turbine noise is characterized by amplitude modulations that are a potential cause of annoyance for wind farm neighbors. One of the possible reasons for the occurrence of strong amplitude modulations at large distances is dynamic stall noise, related to the periodic separation and reattachment of the boundary layer on the wind turbine blade suction side during one rotation [1]. To be able to predict this dynamic stall noise, it is first necessary to develop a model for a static airfoil that accurately captures the evolution of the acoustic pressure spectrum over a wide range of angles of attack. As recently reviewed by Lee *et al.* [2], there exists many theoretical and numerical approaches to predict the trailing edge noise associated with an attached turbulent boundary layer. One of the most popular approach is to consider Amiet's model [3] where the wall pressure spectrum close to the trailing edge is obtained from a semi-empirical model [4–6]. However, when the boundary layer is partially or fully separated, only a few models have been proposed in the literature. One semi-empirical model has been developed by Bertagnolio *et al.* [7], who have shown that Amiet's model still yield reasonable noise predictions at large angles of attack, provided suitable estimates of the wall pressure spectrum Φ_{pp}, the spanwise correlation length l_y and the convection velocity U_c can be obtained.

The objective of the present paper is to combine existing models based on Amiet's theory in order to predict the noise radiated by an airfoil over a large range of angles of attack, for which the boundary layer can be attached or partially separated. Different models are tested to calculate the main inputs of this theory, namely the wall pressure spectrum, the spanwise correlation length and the convection velocity, and the model predictions are compared to measurements recently conducted in the anechoic wind tunnel of Ecole Centrale de Lyon (ECL) [8]. We focus our analysis on a NACA$63_3$418 airfoil of chord $c = 12$ cm at an inflow velocity $U_\infty = 50$ m/s, corresponding to a Reynolds number $Re_c = U_\infty c/\nu = 4.1 \times 10^5$. Note that we exclude from the analysis cases with a fully separated boundary layer at high angles of attack, characterized by a narrow-band peak at low frequency, as shown by Raus *et al.* [8]. For those situations, it would be more appropriate to consider the highly-coherent low-frequency stall noise model proposed by Moreau *et al.* [9].

II. Description of the experimental database

The experiments were conducted in the anechoic wind tunnel of Ecole Centrale de Lyon (ECL). This wind tunnel consists of an open-jet with a rectangular 0.4 m ×0.3 m nozzle exit, followed by two horizontal end-plates guiding

*Assistant Professor, ENSTA Paris, Institute of Mechanical Sciences and Industrial Applications, benjamin.cotte@ensta-paris.fr
†Postdoctoral Researcher, ENSTA Paris, Institute of Mechanical Sciences and Industrial Applications
‡Postdoctoral Researcher, ENSTA Paris, Institute of Mechanical Sciences and Industrial Applications
§Intern, ENSTA Paris, Institute of Mechanical Sciences and Industrial Applications

the incoming flow, as shown in Figure 1. The test section of the wind tunnel is enclosed in an anechoic chamber of dimensions 8 m × 9 m × 10 m. A vertical NACA$63_3$418 airfoil of chord $c = 0.12$ m and of span $s = 0.30$ m was installed between the two end-plates. As shown on Fig. 1, a tripping tape was placed near the leading edge of the airfoil on the pressure side in order to avoid the generation of laminar boundary layer tonal noise [10].

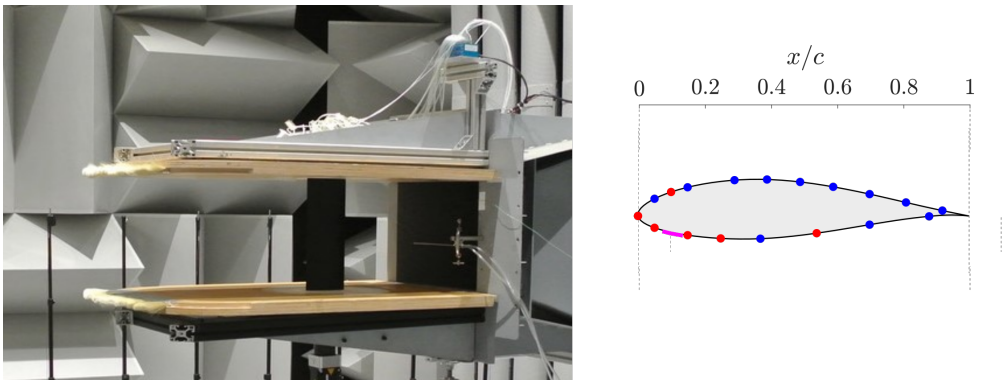

Fig. 1 Picture of the nozzle exit and the end-plates, and position of the pressure taps on the NACA$63_3$418 airfoil. Red dots and blue dots show the positions where only the steady-state surface pressure is measured and the positions where both the steady and fluctuating wall pressures are measured, respectively. Purple areas show the position of the tripping tape.

In order to measure the steady and unsteady wall pressure on the sides of the airfoil, the airfoil was instrumented with 19 steady pressure taps (sampling frequency $f_s = 100$ Hz) and 12 remote-microphone probes ($f_s = 51.2$ kHz), installed mid-span, along the chord of the airfoil (see Fig. 1). Additionally, 5 remote-microphone probes are placed along the span at a distance varying between 3 mm and 30 mm from the mid-span. Far-field noise measurements were performed with one microphone placed in the mid-span, 2 meters away from the airfoil center-chord, and oriented perpendicular to the incoming flow. In order to characterize the background noise generated by the wind tunnel and the end plates, far-field noise measurements are also performed without the airfoil in the test section.

As the measurements are performed in an open wind tunnel, the flow deviates from the nozzle axis due to the lift forces and the effective angle of attack α_e of the airfoil is smaller than the geometric value α_g. In the following, the incidence corrections of Brooks *et al.* [11] are used that yield $\alpha_e \approx \alpha_g/1.55$.

III. Semi-empirical trailing edge noise model based on Amiet's theory

A. Frequency-domain calculation of the far-field acoustic pressure using Amiet's theory

The turbulent boundary layer fluctuations convected at the velocity U_c interact with the trailing edge of an airfoil to generate trailing edge noise. For a fixed airfoil of span L and chord c, the original model proposed by Amiet [3] predicts the noise generated by the trailing edge of a fixed airfoil assimilated to a thin plate interacting with turbulent gusts of uniform velocity. The Power Spectral Density (PSD) of the acoustic pressure due to the TEN produced by an airfoil of large aspect ratio ($L > 3c$) that is observed in the far field (x_R, y_R, z_R) is given by [12]:

$$S_{pp}(x_R, y_R, z_R, \omega) = \left(\frac{kcz_R}{4\pi S_0^2}\right)^2 2L\,\Phi_{pp}(\omega)\,l_y\left(\omega, \frac{ky_R}{S_0}\right)\left|\mathcal{L}_{TE}\left(x_R, \frac{\omega}{U_c}, \frac{ky_R}{S_0}\right)\right|^2, \tag{1}$$

where ω is the angular frequency, k is the acoustic wavenumber, S_0 is the modified distance between the source and the observer, Φ_{pp} is the wall pressure fluctuation spectrum, l_y is the spanwise coherence length, and $\mathcal{L}_{TE}$ is the transfer function for trailing edge noise.

The spanwise coherence length $l_y(\omega, K_y)$ can be obtained experimentally by taking the Fourier transform of the coherence function $\gamma_y^2(\omega, \eta)$ between the pressure signals at two pressure taps whose separation is η along the spanwise direction [7]:

$$l_y(\omega, K_y) = \int_{-\infty}^{\infty} \sqrt{\gamma_y^2(\omega, \eta)} e^{-iK_y\eta} d\eta. \tag{2}$$

For a receiver in the mid-span ($y_R = 0$), the relevant spanwise wavenumber is $K_y = 0$ from Equation (1) and the spanwise coherence length is simply written $l_y(\omega)$.

B. Modeling of the spanwise coherence lengths

1. For attached boundary layers

For an attached boundary layer, various models have been proposed in the literature for the spanwise coherence length, as listed for instance in the article of Hu [13]. In the present study we compare Corcos model [14] and the Smol'yakov and Tkachenko model [15]. In the Corcos model, the spanwise coherence length is written:

$$l_y(\omega) = \frac{b_c U_c}{\omega} \quad \text{with} \quad U_c = \chi U_\infty. \tag{3}$$

In the Smol'yakov and Tkachenko model, the basic form of Corcos model is used but a correction is made to account for the finite size of the boundary layer:

$$l_y(\omega) = \frac{b_c U_c}{\omega} A^{-1} \quad \text{with} \quad A = \sqrt{1 - \frac{\beta U_c}{\omega \delta^*} + \left(\frac{\beta U_c}{\omega \delta^*}\right)^2}, \tag{4}$$

where the convection velocity U_c is deduced from [16]:

$$\frac{U_c}{U_\infty} = \frac{1.6\omega\delta^*/U_\infty}{1 + 16\omega\delta^*/U_\infty} + 0.6, \tag{5}$$

and with δ^* the displacement thickness. In the present study, we use $b_c = 1.47$ and $\chi = 0.7$ for the Corcos model, and $b_c = 1.25$ and $\beta = 0.25$ for the Smol'yakov model.

2. For partially separated boundary layers

Bertagnolio *et al.* [7] propose a model for the spanwise coherence function based on the streamwise correlation length L_x, that tends to increase when the separation point x_{sep} moves away from the trailing edge. They show that the correlation length increases roughly linearly as a function of the distance from the separation point $x - x_{\text{sep}}$. For Reynolds numbers lower than 1.6×10^6, they obtain the following scaling law:

$$L_x(x) \approx 0.13(x - x_{\text{sep}}) Re_M^{1/4}, \tag{6}$$

with $Re_M = Re_c/10^6$ the reduced Reynolds number.

The spanwise coherence length is finally written [7, 17]:

$$l_y(\omega) = \frac{L_x}{\pi \left[a_y(St_L - St_y)^2 + b_y\right]} \quad \text{with} \quad St_L = \frac{f L_x}{U_\infty}. \tag{7}$$

Based on wall pressure measurements at $x/c = 0.975$ on a NACA64-618 airfoil, Bertagnolio *et al.* [7] obtain the coefficients $St_y = 0.103$, $a_y = 70.1$ and $b_y = 0.350$.

C. Wall pressure spectral models for attached and partially separated boundary layers

1. For attached boundary layers

When the boundary layer is attached, the wall pressure spectrum on the suction side depends on the strength of the adverse pressure gradient, and can be calculated with Lee's semi-empirical model [6], which is an extension of Rozenberg's model [5]. The input parameters of this model are the external velocity U_e, the displacement thickness δ^*, the wall shear stress τ_w, and Clauser's parameter $\beta_C = \frac{\theta}{\tau_w}\frac{dp}{dx}$, where θ is the momentum thickness and $\frac{dp}{dx}$ is the pressure gradient. These parameters can be estimated from an Xfoil calculation in order to predict the wall pressure spectrum at the same chordwise position as in the experimental setup.

Rozenberg-Lee's model has been validated for adverse pressure gradient until $\beta_C \approx 30$. When the pressure gradient is favorable ($\beta_C < 0$), this model cannot be used and Goody's model [4] that has been developed for a zero pressure gradient boundary layer is considered.

2. For partially separated boundary layers

Bertagnolio *et al.* [7] propose a model for the wall pressure spectrum of a partially separated boundary layer, based on the streamwise correlation length L_x already used in Section III.B.2. Different scaling laws are obtained depending on the frequency range, based on the Strouhal numbers $St_L = fL_x/U_\infty$ and $St_S = f(x - x_{\text{sep}})/U_\infty$. Using Equation (6), it can be noticed that these two Strouhal numbers are related by:

$$St_L = \frac{fL_x}{U_\infty} \approx 0.13 \frac{f(x - x_{\text{sep}})}{U_\infty} Re_M^{1/4} = 0.13 Re_M^{1/4} St_S, \tag{8}$$

so $St_L \approx 0.10 St_S$ for $Re_M = 0.41$.

Focusing on Reynolds numbers lower than 1.6×10^6, Bertagnolio *et al.* obtain the following wall pressure model [7, 17]:

$$\phi_{pp}(f) = \begin{cases} \frac{q_\infty^2 L_x}{U_\infty} c_B \sqrt{St_L} & \text{for} \quad St_L < 0.02, \\ \frac{q_\infty^2 L_x}{U_\infty} \frac{5\times10^{-7} St_L}{3\times10^{-6} + St_L^5} & \text{for} \quad St_L > 0.02 \quad \text{and} \quad St_S < 2, \\ \frac{q_\infty^2 (x - x_{\text{sep}})}{U_\infty} \frac{5\times10^{-4}}{St_c^2} & \text{for} \quad St_S > 2, \end{cases} \tag{9}$$

with $St_c = fc/U$, $q_\infty = 0.5\rho U_\infty^2$, ρ the air density, and where c_B is chosen so that the model is continuous at $St_L = 0.02$:

$$c_B \sqrt{0.02} = \frac{5 \times 10^{-7} \times 0.02}{3 \times 10^{-6} + 0.02^5}. \tag{10}$$

IV. Results

A. Boundary layer characterization and angle of attack correction

The lift coefficient C_L is estimated by integrating the steady surface pressure along the airfoil chord and is presented in Figure 2(a). At high angles of attack, a plateau is present in the pressure coefficient on the suction side, as can be seen in Figure 3(b-d), that corresponds to the separation of the boundary layer. The separation point x_{sep} can thus be estimated from the surface pressure measurements, as shown in Figure 2(b). As there is a finite number of pressure taps on the suction side, there is an uncertainty associated with these estimates, plotted as solid lines in Figure 2(b). According to these estimates, the boundary layer is partially separated for $\alpha_g \in [15°, 24°]$, and completely separated for $\alpha_g \geq 25°$. As the two last pressure taps are located at $x/c = 81\%$ and 92%, it is not possible to estimate boundary layer separation between $x/c = 81\%$ and the trailing edge using this method.

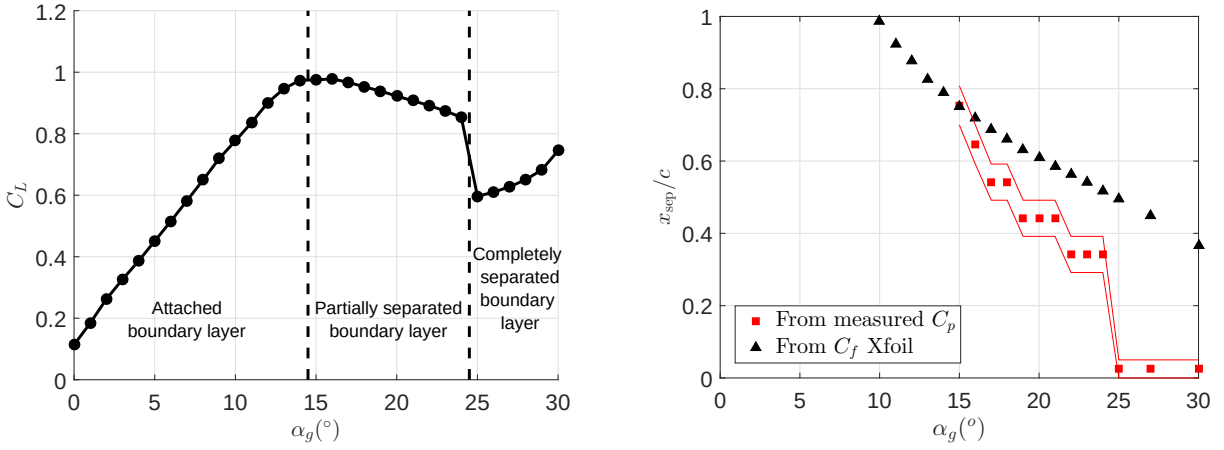

Fig. 2 (a) Lift coefficient and (b) position of the separation point estimated from the measurements of the pressure coefficient C_p or from the Xfoil calculation of the friction coefficient C_f.

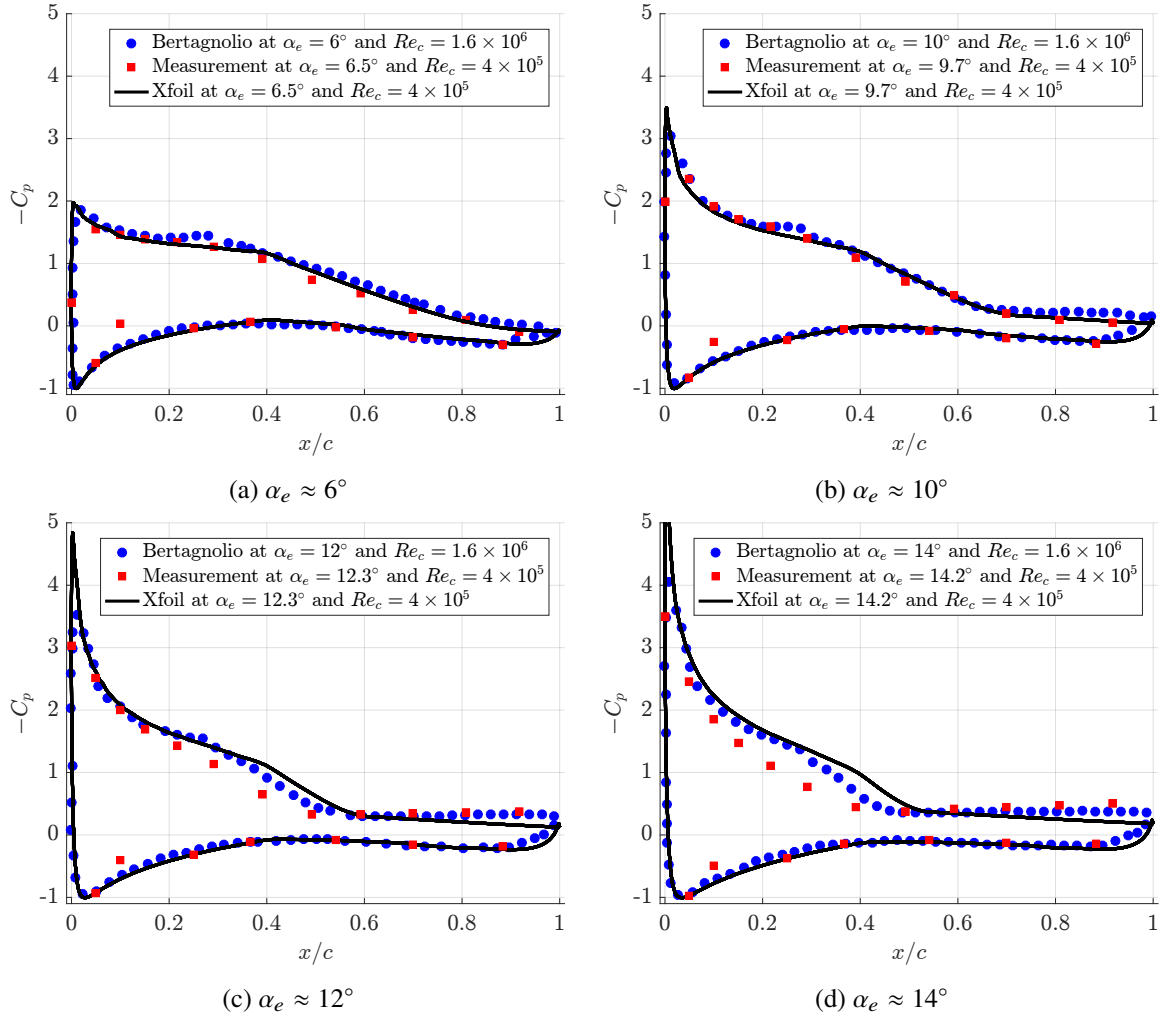

(a) $\alpha_e \approx 6°$ (b) $\alpha_e \approx 10°$

(c) $\alpha_e \approx 12°$ (d) $\alpha_e \approx 14°$

Fig. 3 Pressure coefficient distribution measured by Bertagnolio *et al.* [7] at $Re_c = 1.6 \times 10^6$, measured in the ECL anechoic wind tunnel at $Re_c = 4 \times 10^5$, and calculated with Xfoil at $Re_c = 4 \times 10^5$.

The separation point x_{sep} can also be estimated from an Xfoil calculation, by looking at the region where the friction coefficient C_f is negative. First, the distribution of the pressure coefficient C_p calculated by Xfoil is compared to measurements in Figure 3, in order to assess the validity of the angle of attack correction. It can be seen that the Xfoil calculations are in excellent agreement with measurements at relatively low angles of attack ($\alpha_e = 6°$ and $10°$). The agreement is less good on the suction side at higher angles of attack, where it appears that the separation point is too close to the trailing edge in the Xfoil calculation, as can be seen in Figure 2(b) too. This discrepancy can be due to the inaccuracy of the angle of attack correction, but also to the fact that Xfoil is not accurate anymore in the presence of massive boundary layer separation. Note that our measurements are relatively close to the measurements performed by Bertagnolio *et al.* [7] at a higher Reynolds number ($Re_c = 1.6 \times 10^6$).

The main boundary layer parameters calculated by Xfoil are given in Table 1 for $x/c = 92\%$ and $x/c = 99\%$ on the suction side. The position $x/c = 92\%$ corresponds to the pressure tap that is closest to the trailing edge, and $x/c = 99\%$ is the position that will be used for the far-field acoustic pressure calculations, following Lee and Shum [18]. It appears that the boundary layer thickness increases with the angle of attack, as well as the shape factor $H = \delta^*/\theta$. The friction coefficient C_f approaches zero when $\alpha_g = 10°$, corresponding to high values of the Clauser's parameter β_C, for which the Rozenberg-Lee's model is not valid anymore. The same type of information is also given in Table 1 on the pressure side, where the pressure tap at $x/c = 88\%$ is closest to the trailing edge. It appears that the pressure gradient is slightly positive at $x/c = 88\%$, which allows us to use the Rozenberg-Lee's model, but is negative at $x/c = 99\%$, which

Table 1 Boundary layer parameters calculated by Xfoil on the suction side at $x/c = 92\%$ (black) and 99% (blue), and on the pressure side at $x/c = 88\%$ (black) and 99% (blue)

	suction side				pressure side			
	δ^* (mm)	$H = \delta^*/\theta$	$C_f(\times 10^{-3})$	β_C	δ^* (mm)	$H = \delta^*/\theta$	$C_f(\times 10^{-3})$	β_C
$\alpha_g = 2°$	0.78	1.74	1.96	3.39	0.55	1.60	2.25	1.82
$\alpha_e = 1.3°$	1.14	1.93	1.16	10.54	0.52	1.47	2.79	-3.75
$\alpha_g = 4°$	0.87	1.79	1.80	4.11	0.50	1.59	2.33	1.58
$\alpha_e = 2.6°$	1.27	1.99	1.02	11.99	0.47	1.45	3.00	-3.74
$\alpha_g = 6°$	0.99	1.85	1.56	5.26	0.46	1.57	2.42	1.37
$\alpha_e = 3.9°$	1.46	2.10	0.83	14.39	0.42	1.43	3.20	-3.61
$\alpha_g = 8°$	1.70	2.26	0.69	13.06	0.42	1.56	2.57	1.07
$\alpha_e = 5.2°$	2.41	2.65	0.29	27.50	0.36	1.40	3.69	-3.64
$\alpha_g = 10°$	2.90	3.11	0.098	51.48	0.38	1.54	2.80	0.77
$\alpha_e = 6.5°$	3.87	3.84	0	inf	0.29	1.36	4.42	-3.42

constrains us to consider Goody's model.

B. Spanwise coherence length

When the boundary layer is attached, we compare in Figure 4(a-b) the spanwise coherence length calculated with the models of Corcos or Smol'yakov to the one estimated from coherence measurements. In the experimental estimates, we have discarded results when the coherence function is smaller than 0.1 at the smallest spanwise distance $\eta = 3$ mm, which explains that there are missing values. As expected, both models agree at high frequencies, and are in good agreement with measurements above $St_c = 4$. Below this value, the Smol'yakov model that accounts for the finite size of the boundary layer follows relatively well the measured values.

When the boundary layer is partially separated, the spanwise coherence increases significantly for St_c below 4, and Corcos model cannot be used anymore, as can be seen in Figure 4(c-f). Bertagnolio's model that depends on the separation point x_{sep} predicts relatively well the frequency at which l_y is maximum, especially when x_{sep} is estimated from C_p measurements, but the value of l_y is significantly underpredicted. In order to correct this behavior, we modified the value of the coefficient b_y in Bertagnolio's model. Indeed, it appears from Equation (7) that the maximum value of l_y is $L_x/\pi b_y$ at $St_L = St_y$. A better fit is obtained by replacing $b_y = 0.350$ by $b_y = 0.08$, as seen in Figure 4(c-f), although the behavior at low frequencies ($St_L < St_y$) is not satisfactory. More work is needed to understand if this discrepancy compared to Bertagnolio's results is due to a difference in the Reynolds number considered, and/or to the difference in the airfoil shape.

C. Wall pressure spectra

Let us consider first the wall pressure PSD at low angles of attack, for which the boundary layer is attached. Figure 5 shows that the Rozenberg-Lee model underestimates the measured spectra, especially on the pressure side where the difference is greater than 5 dB. On the suction side, the underprediction is less severe and the predicted values are 3 to 4 dB lower than the measurements for $fc/U > 4$.

When the boundary layer is partially separated, we consider Bertagnolio's model with the separation point x_{sep} obtained either from the pressure coefficient measurements or from the friction coefficient calculated with Xfoil. Figure 6 shows that Bertagnolio's model captures quite well the maximum of the wall pressure spectrum when x_{sep} is estimated from the measured C_p. Bertagnolio's model predicts a spectral maximum at $St_L \approx 0.06$, which means that the associated Strouhal number $St_c = St_L/(L_x/c)$ decreases as the angle of attack increases, as L_x is proportional to $x - x_{\text{sep}}$. At frequencies above the peak, however, the model tends to overestimate the measured spectrum. When the separation point is estimated from the Xfoil calculation, the correlation length L_x is too small because the separated region is underestimated, which explain why the spectral peak is shifted to higher frequencies.

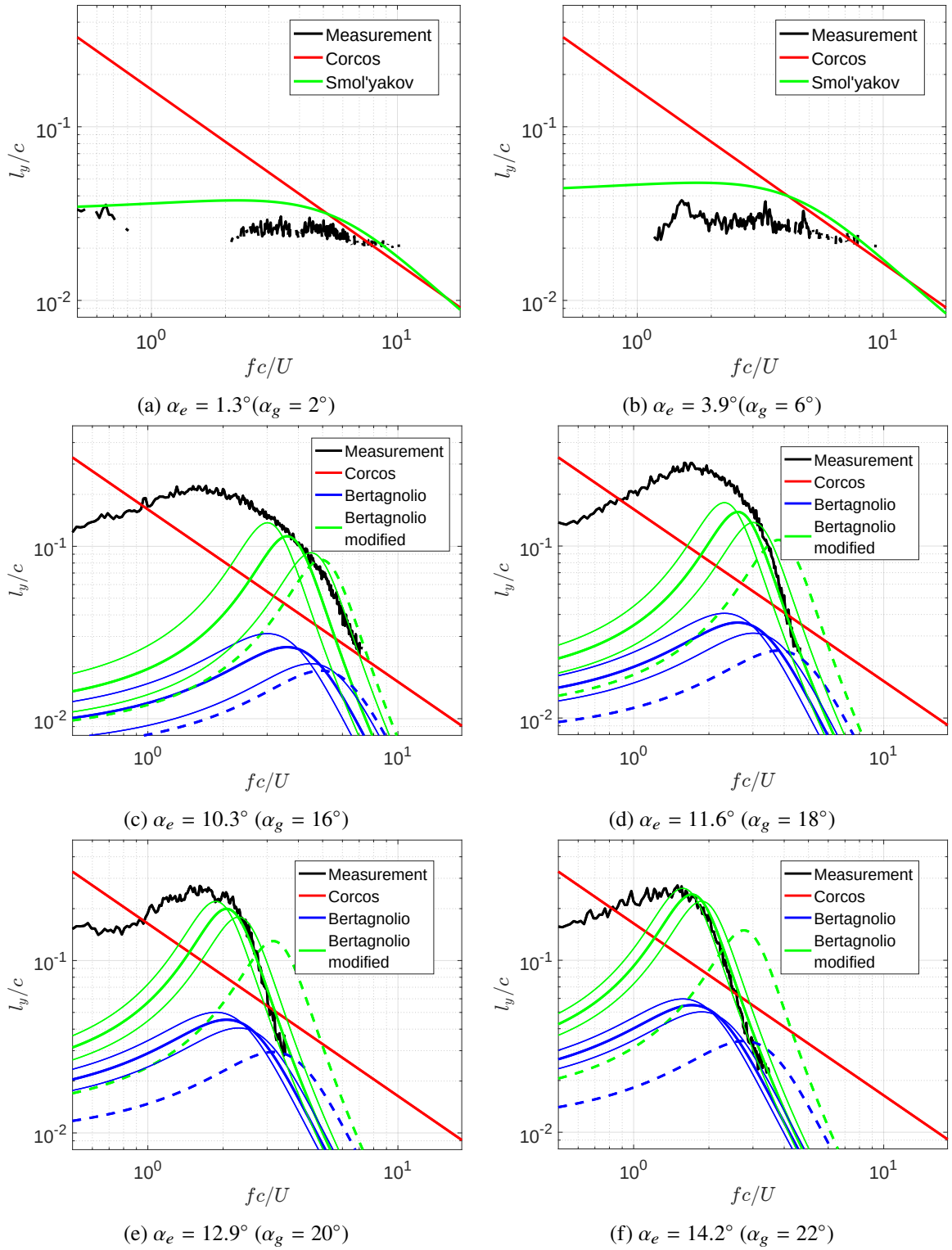

(a) $\alpha_e = 1.3°(\alpha_g = 2°)$

(b) $\alpha_e = 3.9°(\alpha_g = 6°)$

(c) $\alpha_e = 10.3°$ $(\alpha_g = 16°)$

(d) $\alpha_e = 11.6°$ $(\alpha_g = 18°)$

(e) $\alpha_e = 12.9°$ $(\alpha_g = 20°)$

(f) $\alpha_e = 14.2°$ $(\alpha_g = 22°)$

Fig. 4 Spanwise coherence length with respect to $St_c = fc/U$ at various angles of attack. In subplots (c-f), Bertagnolio's model is plotted with a thick solid line when the separation point is estimated from the C_p measurements, and with a thick dashed line when the separation point is estimated from the Xfoil calculation. The thin solid lines correspond to the uncertainty on the value of the separation point estimated from the C_p measurements.

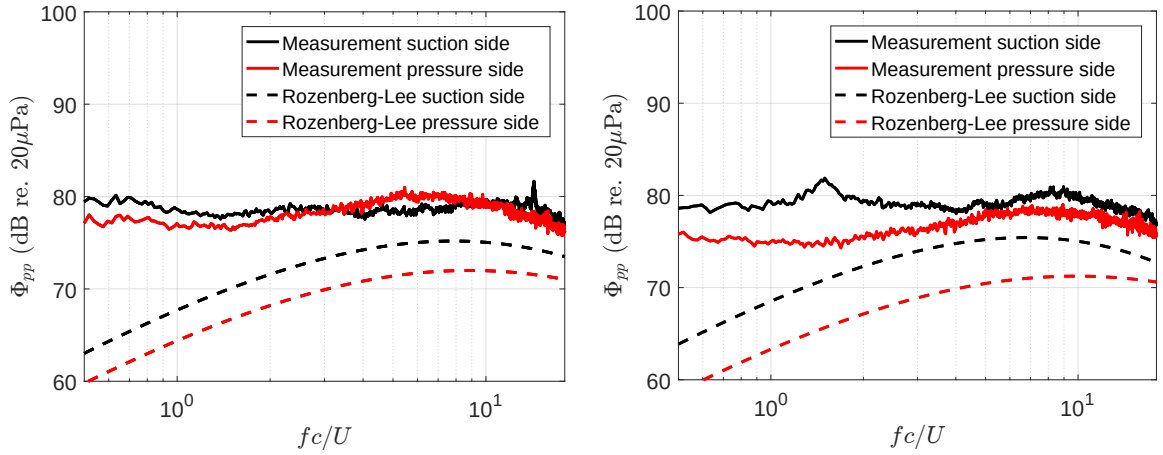

(a) $\alpha_e = 1.3°$ ($\alpha_g = 2°$) (b) $\alpha_e = 3.9°$ ($\alpha_g = 6°$)

Fig. 5 Wall pressure PSD at $x/c = 92\%$ on the suction side, and at $x/c = 88\%$ on the pressure side.

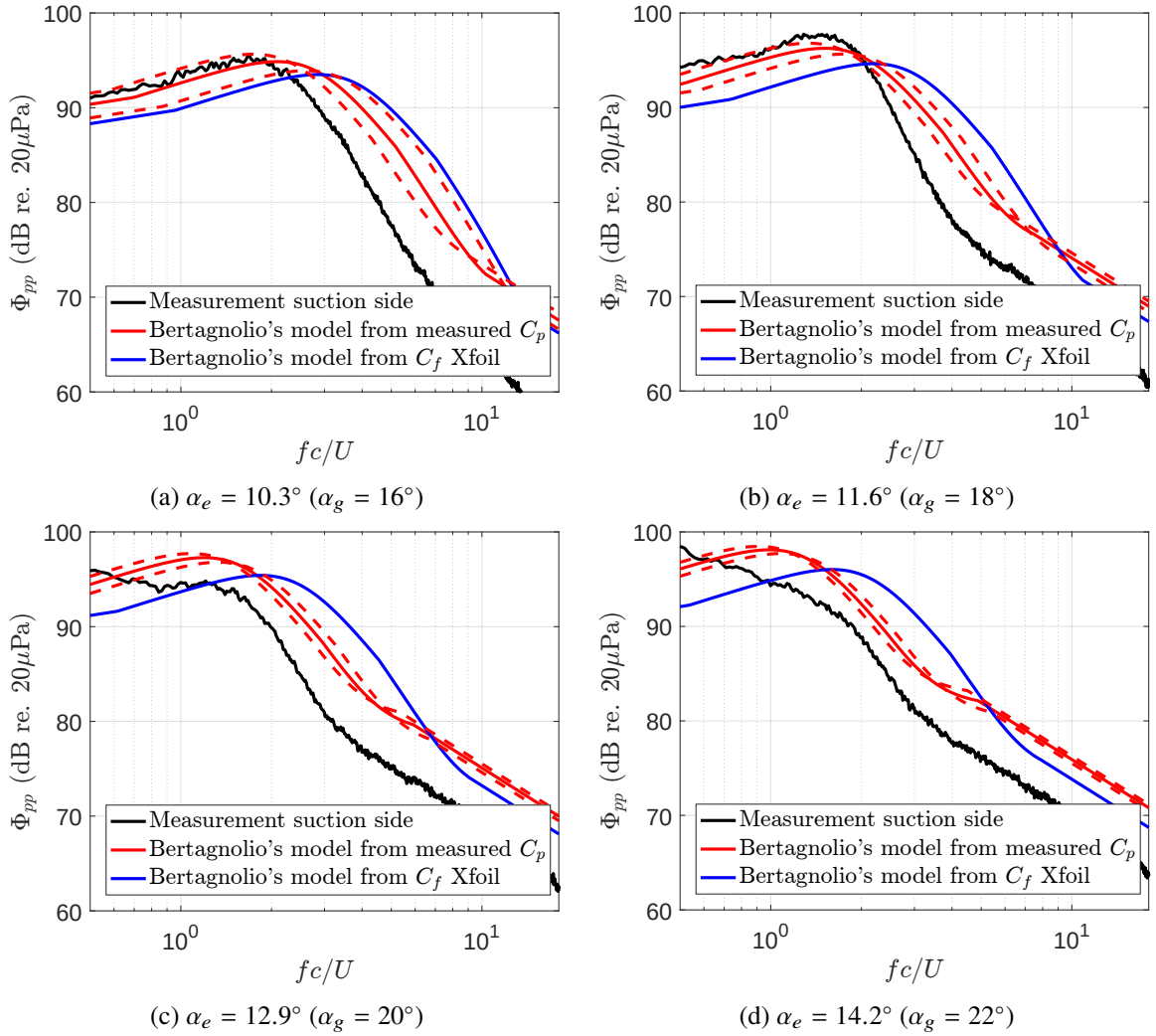

(a) $\alpha_e = 10.3°$ ($\alpha_g = 16°$) (b) $\alpha_e = 11.6°$ ($\alpha_g = 18°$)

(c) $\alpha_e = 12.9°$ ($\alpha_g = 20°$) (d) $\alpha_e = 14.2°$ ($\alpha_g = 22°$)

Fig. 6 Wall pressure PSD with respect to $St_c = fc/U$ for $Re_c = 4.1 \times 10^5$. The red dashed lines correspond to the uncertainty on the value of the separation point estimated from the C_p measurements.

To obtain a synthetic comparison between model predictions and measurements, Figure 7 plots the wall pressure spectrum as a function of the Strouhal number $St_c = fc/U_\infty$ and the effective angle of attack α_e. Note that Lee's model cannot be calculated above $\alpha_e = 6.5°$ as Xfoil predicts a negative value of the friction coefficient at $x/c = 92\%$, which corresponds to a separated boundary layer. As already seen in Figure 5, the Rozenberg-Lee's underpredicts the measured spectrum, but is in relatively good agreement for $St_c > 4$. When the separation point is estimated from the C_p measurements, Bertagnolio's model accurately predicts the spectral evolution at low frequencies ($St_c < 3$), but tends to overestimate the spectral values at higher frequencies. Note that Bertagnolio's model cannot be used below 9° at $x/c = 92\%$ as the separation point location is too close to the trailing edge ($x < x_{sep}$ thus $L_x < 0$).

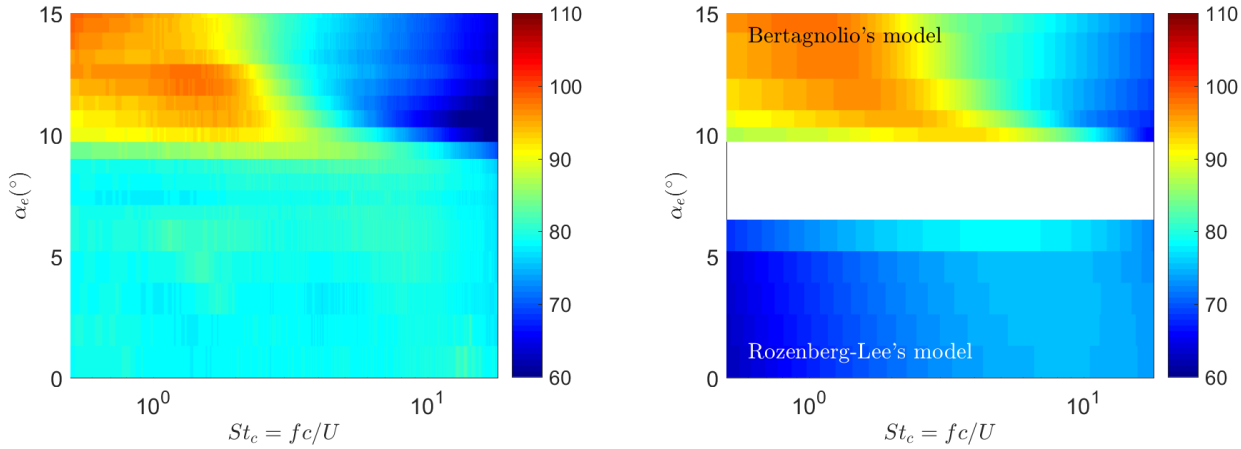

Fig. 7 (a) Measured and (b) predicted wall pressure PSD in dB re. $(20\mu\text{Pa})^2$/Hz at $x/c = 92\%$ on the suction side with respect to $St_c = fc/U_\infty$ and to effective angles of attack α_e between 0 and 15° at $Re_c = 4.1 \times 10^5$.

D. Far-field acoustic pressure

In this section, we compare the predictions for the PSD of acoustic pressure obtained from Amiet's theory, as given by Equation (1), to measurements in the mid-span, using different models for the spanwise coherence $l_y(\omega)$ and the wall pressure spectrum $\Phi_{pp}(\omega)$, both calculated at $x/c = 99\%$. As already shown in [8], the signal-to- noise ratio is relatively small at low angles of attack, thus we choose here to plot the PSD of far-field acoustic pressure with background noise substracted, and we discard the data if the total noise does not exceed the background noise by at least 2 dB. First, for an attached boundary layer, predictions obtained with the models of Corcos or Smol'yakov for the spanwise coherence length are compared to the measurements in Figure 8(a-b). The Rozenberg-Lee model is used on the suction side, and Goody's model is considered on the pressure side, as $\beta_C < 0$ at $x/c = 99\%$. The model predictions are in good agreement with the measurements at high frequencies ($fc/U > 4$), but underestimate the measurements at lower frequencies, which can be attributed to the under-prediction of the wall pressure spectrum observed in Figure 5. Smol'yakov model for the spanwise coherence length provides a slightly better agreement with measurements than Corcos model, with a difference of 2 dB at $fc/U \approx 4$.

Figure 8(c-f) shows the comparison between model predictions and measurements at higher angles of attack. As seen before, the spectral peak is well predicted by Bertagnolio's model when the separation point is estimated from the C_p measurements. When the modified Bertagnolio's model for the spanwise coherence length is used, the spectral amplitudes at low frequencies are better predicted, except at $\alpha_e = 14.2°$ where the wall pressure spectrum becomes less peaky, as can be seen in Figure 6(d).

V. Conclusion

In this study, we have proposed a semi-empirical trailing edge noise model based on Amiet's theory that can be applied to both attached and partially separated boundary layers. We have not considered cases with fully separated boundary layers that can occur at very large angles of attack. The model predictions are compared to experimental results

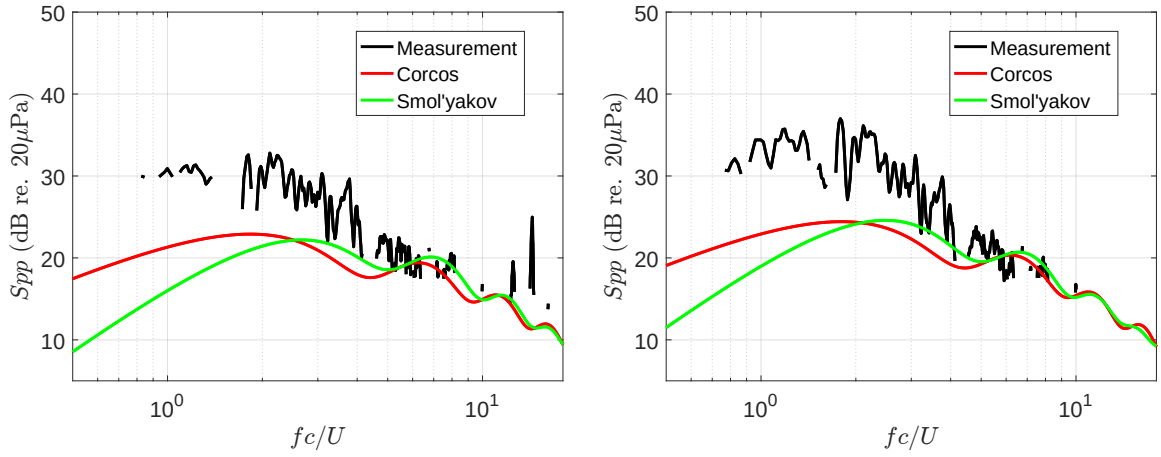

(a) $\alpha_e = 1.3°$ ($\alpha_g = 2°$)

(b) $\alpha_e = 3.9°$ ($\alpha_g = 6°$)

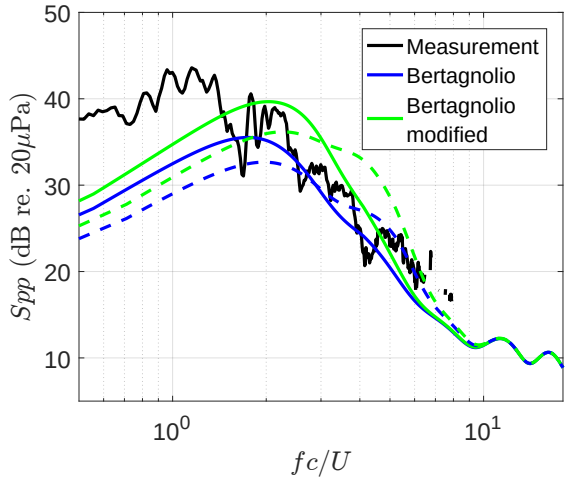

(c) $\alpha_e = 10.3°$ ($\alpha_g = 16°$)

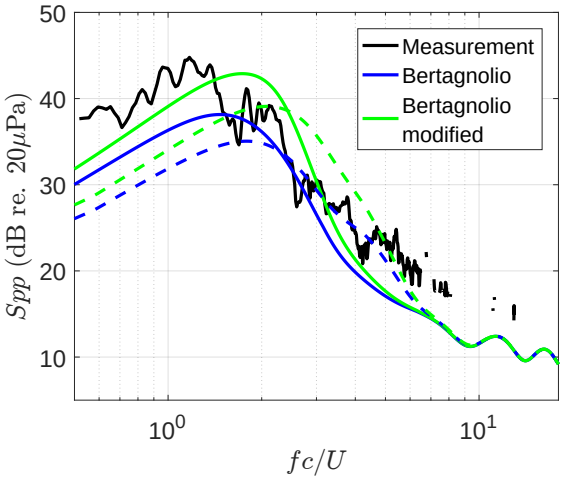

(d) $\alpha_e = 11.6°$ ($\alpha_g = 18°$)

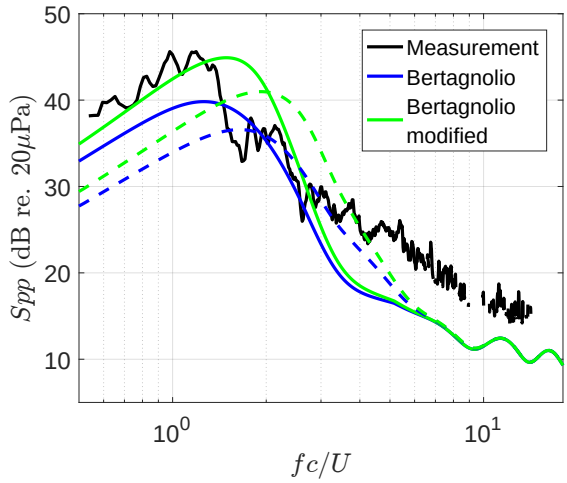

(e) $\alpha_e = 12.9°$ ($\alpha_g = 20°$)

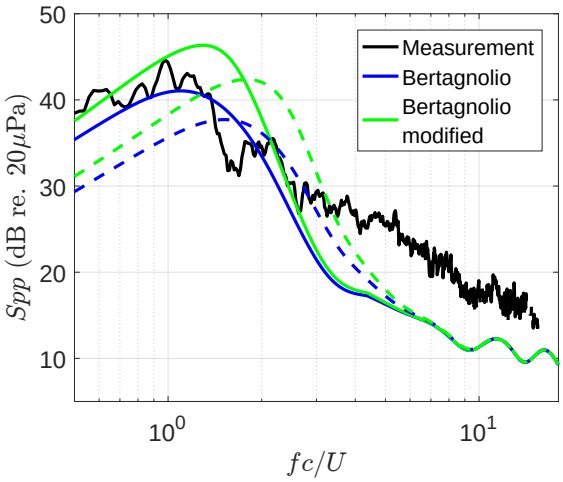

(f) $\alpha_e = 14.2°$ ($\alpha_g = 22°$)

Fig. 8 Acoustic pressure PSD with respect to $St_c = fc/U$ obtained with different spanwise coherence length models. In subplots (c-f), Bertagnolio's model is plotted with a solid line when the separation point is estimated from the C_p measurements, and with a dashed line when the separation point is estimated from the Xfoil calculation.

acquired on a NACA$63_3$418 airfoil in the anechoic wind tunnel of the École Centrale de Lyon at a Reynolds number based on the chord of 4.1×10^5. As the measurements are performed in an open wind tunnel, we have first validated the angle of attack correction of Brooks by comparing the pressure coefficient distribution predicted by Xfoil with the measured values. The agreement is excellent at low angles of attack, but Xfoil calculations tend to underestimate the length of the separation region at higher angles of attack.

We have then considered the two main input parameters of Amiet's theory, i.e. the spanwise coherence length and the wall pressure spectrum. For an attached boundary layer, the Smol'yakov model can be used to estimate the spanwise coherence length over a large frequency range. The Rozenberg-Lee model tends to underestimate the measured wall pressure spectrum, but yields relatively good results on the suction side for $St_c > 4$. For a partially separated boundary layer, Bertagnolio's model predicts quite well the frequency at which the spanwise coherence length is maximum when the separation point is estimated from the measured distribution of the pressure coefficient, but underestimates its value. It also provides an accurate prediction of the wall pressure spectrum at $St_c < 3$. The far-field acoustic pressure predictions are seen to follow the measurements in the frequency range of validity of the models for the spanwise coherence length and for the wall pressure spectrum.

In order to obtain a prediction model that is accurate over a large range of angles of attack, it seems utterly important to estimate reliably the separation point. As Xfoil seems to underestimate the length of the separated region, it might be interesting in the future to use a RANS simulation to estimate the separation point. Also, some work is needed to predict the evolution of the spanwise coherence length and of the wall pressure spectrum at intermediate angles of attack, where none of the models are reliable.

Acknowledgments

This research is funded by the French National Agency for Research under grant agreement N°ANR-19-CE36-0009 and by the Agence Innovation Défense under grant agreement N°2018 60 0071 00 470 75 01.

References

[1] Oerlemans, S., "Effect of wind shear on amplitude modulation of wind turbine noise," *International Journal of Aeroacoustics*, Vol. 14, 2015, pp. 715–728.

[2] Lee, S., Ayton, L., Bertagnolio, F., Moreau, S., Chong, T. P., and Joseph, P., "Turbulent boundary layer trailing-edge noise: Theory, computation, experiment, and application," *Progress in Aerospace Sciences*, Vol. 126, 2021, p. 100737. https://doi.org/10.1016/j.paerosci.2021.100737.

[3] Amiet, R., "Noise Due to Turbulent Flow Past a Trailing Edge," *Journal of Sound and Vibration*, Vol. 47, 1976, pp. 387–393.

[4] Goody, M., "Empirical spectral model of surface pressure fluctuations." *AIAA Journal*, Vol. 42, 2004, pp. 1788–1794.

[5] Rozenberg, Y., Robert, G., and Moreau, S., "Wall-pressure spectral model including the adverse pressure gradient effects," *AIAA Journal*, 2012, pp. 2168–2179.

[6] Lee, S., "Empirical Wall-Pressure Spectral Modeling for Zero and Adverse Pressure Gradient Flows," *AIAA Journal*, Vol. 56, No. 5, 2018, pp. 1818–1829. https://doi.org/10.2514/1.J056528.

[7] Bertagnolio, F., Madsen, H., Fischer, A., and Bak, C., "A semi-empirical airfoil stall noise model based on surface pressure measurements," *Journal of Sound and Vibration*, Vol. 387, 2017, pp. 127–162. https://doi.org/10.1016/j.jsv.2016.09.033.

[8] Raus, D., Cotté, B., Monchaux, R., Sicard, L., Jondeau, E., Souchotte, P., and Roger, M., "Experimental characterization of the noise generated by an airfoil oscillating above stall," *AIAA AVIATION 2021 FORUM*, 2021. https://doi.org/10.2514/6.2021-2291.

[9] Moreau, S., Roger, M., and Christophe, J., "Flow Features and Self-Noise of Airfoils Near Stall or in Stall," *15th AIAA/CEAS Aeroacoustics Conference (30th AIAA Aeroacoustics Conference)*, 2009. https://doi.org/10.2514/6.2009-3198.

[10] Brooks, T. F., Pope, D., and Marcolini, M., "Airfoil self-noise and prediction," 1989.

[11] Brooks, T. F., Marcolini, M., and Pope, D., "Airfoil trailing edge flow measurements and comparison with theory, incorporating open wind tunnel corrections," *9th Aeroacoustics Conference*, 1984. https://doi.org/10.2514/6.1984-2266.

[12] Roger, M., and Moreau, S., "Extensions and limitations of analytical airfoil broadband noise models," *International Journal of Acoustics*, Vol. 9, No. 3, 2010, pp. 273–305.

[13] Hu, N., "Coherence of wall pressure fluctuations in zero and adverse pressure gradients," *Journal of Sound and Vibration*, Vol. 511, 2021. https://doi.org/10.1016/j.jsv.2021.116316.

[14] Corcos, G., "The structure of the turbulent pressure field in boundary layer flows," *Journal of Fluid Mechanics*, Vol. 18, 1964, p. 353–378.

[15] Smol'yakov, A., and Tkachenko, V., "Model of a field of pseudosonic turbulent wall pressures and experimental data," *Akust. Zh.*, Vol. 37, 1991, pp. 1199–1207.

[16] Smol'yakov, A., "A new model for the cross spectrum and wavenumber-frequency spectrum of turbulent pressure fluctuations in a boundary layer," *Acoust. Phys.*, Vol. 52, 2006, pp. 331–337.

[17] Bertagnolio, F., Madsen, H., Fischer, A., and Bak, C., "Corrigendum to "A semi-empirical airfoil stall noise model based on surface pressure measurements" [J. Sound Vib. 387 (2017) 127–162]," *Journal of Sound and Vibration*, Vol. 424, 2018, p. 378. https://doi.org/10.1016/j.jsv.2018.01.053.

[18] Lee, S., and Shum, J., "Prediction of Airfoil Trailing-Edge Noise Using Empirical Wall-Pressure Spectrum Models," *AIAA Journal*, Vol. 57, No. 3, 2019. https://doi.org/10.2514/1.J057787.